# Coupled $Ca^{2+}/H^+$ transport by cytoplasmic buffers regulates local $Ca^{2+}$ and $H^+$ ion signaling

Pawel Swietach[a], Jae-Boum Youm[a,b], Noriko Saegusa[c], Chae-Hun Leem[d], Kenneth W. Spitzer[c], and Richard D. Vaughan-Jones[a,1]

[a]Burdon Sanderson Cardiac Science Centre, Department of Physiology, Anatomy, and Genetics, Oxford University, Oxford OX1 3PT, United Kingdom; [b]Department of Physiology and Biophysics, College of Medicine, Inje University, Inje 621-749, Korea; [c]Nora Eccles Harrison Cardiovascular Research and Training Institute, University of Utah, Salt Lake City, UT; and [d]Department of Physiology, University of Ulsan College of Medicine, Seoul, Korea

Edited by David E. Clapham, Howard Hughes Medical Institute, Children's Hospital Boston, Boston, MA, and approved April 18, 2013 (received for review December 21, 2012)

**$Ca^{2+}$ signaling regulates cell function. This is subject to modulation by $H^+$ ions that are universal end-products of metabolism. Due to slow diffusion and common buffers, changes in cytoplasmic $[Ca^{2+}]$ ($[Ca^{2+}]_i$) or $[H^+]$ ($[H^+]_i$) can become compartmentalized, leading potentially to complex spatial $Ca^{2+}/H^+$ coupling. This was studied by fluorescence imaging of cardiac myocytes. An increase in $[H^+]_i$, produced by superfusion of acetate (salt of membrane-permeant weak acid), evoked a $[Ca^{2+}]_i$ rise, independent of sarcolemmal $Ca^{2+}$ influx or release from mitochondria, sarcoplasmic reticulum, or acidic stores. Photolytic $H^+$ uncaging from 2-nitrobenzaldehyde also raised $[Ca^{2+}]_i$, and the yield was reduced following inhibition of glycolysis or mitochondrial respiration. $H^+$ uncaging into buffer mixtures in vitro demonstrated that $Ca^{2+}$ unloading from proteins, histidyl dipeptides (HDPs; e.g., carnosine), and ATP can underlie the $H^+$-evoked $[Ca^{2+}]_i$ rise. Raising $[H^+]_i$ tonically at one end of a myocyte evoked a local $[Ca^{2+}]_i$ rise in the acidic microdomain, which did not dissipate. The result is consistent with uphill $Ca^{2+}$ transport into the acidic zone via $Ca^{2+}/H^+$ exchange on diffusible HDPs and ATP molecules, energized by the $[H^+]_i$ gradient. $Ca^{2+}$ recruitment to a localized acid microdomain was greatly reduced during intracellular $Mg^{2+}$ overload or by ATP depletion, maneuvers that reduce the $Ca^{2+}$-carrying capacity of HDPs. Cytoplasmic HDPs and ATP underlie spatial $Ca^{2+}/H^+$ coupling in the cardiac myocyte by providing ion exchange and transport on common buffer sites. Given the abundance of cellular HDPs and ATP, spatial $Ca^{2+}/H^+$ coupling is likely to be of general importance in cell signaling.**

calcium | heart | mobile buffer | pH | dual microperfusion

Most cells are exquisitely responsive to calcium ($Ca^{2+}$) (1) and hydrogen ($H^+$) ions (i.e., pH) (2). In cardiac myocytes, $Ca^{2+}$ ions trigger contraction and control growth and development (3), whereas $H^+$ ions, which are generated or consumed metabolically, are potent modulators of essentially all biological processes (4). By acting on $Ca^{2+}$-handling proteins directly or via other molecules, $H^+$ ions exert both inhibitory and excitatory effects on $Ca^{2+}$ signaling. For example, in the ventricular myocyte, $H^+$ ions can reduce $Ca^{2+}$ release from sarcoplasmic reticulum (SR) stores, through inhibition of the SR $Ca^{2+}$ ATPase (SERCA) pump and ryanodine receptor (RyR) $Ca^{2+}$ channels (5, 6). In contrast, $H^+$ ions can enhance SR $Ca^{2+}$ release by stimulating sarcolemmal $Na^+/H^+$ exchange (NHE), which raises intracellular $[Na^+]$ and reduces the driving force for $Ca^{2+}$ extrusion on $Na^+/Ca^{2+}$ exchange (NCX), leading to cellular retention of $Ca^{2+}$ (7, 8). $Ca^{2+}$ signaling is thus subservient to pH.

Cytoplasmic $Ca^{2+}$ and $H^+$ ions bind avidly to buffer molecules, such that <1% of all $Ca^{2+}$ ions and <0.001% of all $H^+$ ions are free. Some of these buffers bind $H^+$ and $Ca^{2+}$ ions competitively, and this has been proposed to be one mechanism underlying cytoplasmic $Ca^{2+}/H^+$ coupling (9). Reversible binding to buffers greatly reduces the effective mobility of $Ca^{2+}$ and $H^+$ ions in cytoplasm (10, 11) and can allow for highly compartmentalized ionic microdomains, and hence a spatially heterogeneous regulation of cell function. In cardiac myocytes under resting (diastolic) conditions, the cytoplasm-averaged concentration of free $[Ca^{2+}]$ ($[Ca^{2+}]_i$) and $[H^+]$ ($[H^+]_i$) ions is kept near $10^{-7}$ M by membrane transporter proteins. Thus, $[H^+]_i$ is regulated by the balance of flux among acid-extruding and acid-loading transporter proteins at the sarcolemma [e.g., NHE and $Cl^-/OH^-$ (CHE) exchangers, respectively] (4). Similarly, the activity of SERCA and NCX proteins returns $[Ca^{2+}]_i$ to its diastolic level after evoked signaling events (3, 12). Despite these regulatory mechanisms, cytoplasmic gradients of $[H^+]_i$ and $[Ca^{2+}]_i$ do occur in myocytes and are an important part of their physiology. Gradients arise from local differences in transmembrane fluxes that alter $[H^+]_i$ or $[Ca^{2+}]_i$. For example, spatial $[H^+]_i$ gradients are produced when NHE transporters, expressed mainly at the intercalated disk region, are activated (4, 13) or when membrane-permeant weak acids, such as $CO_2$, are presented locally (14). Similarly, release of $Ca^{2+}$ through a cluster of RyR channels in the SR produces $[Ca^{2+}]_i$ nonuniformity in the form of $Ca^{2+}$ sparks (15). Given the propensity of cytoplasm to develop ionic gradients, it is important to understand their underlying mechanism and functional role.

The present work demonstrates a distinct form of spatial interaction between $Ca^{2+}$ and $H^+$ ions. We show that cytoplasmic $[H^+]$ gradients can produce stable $[Ca^{2+}]_i$ gradients, and vice versa, and that this interaction is mediated by low-molecular-weight (mobile) buffers with affinity for both ions. We demonstrate that the diffusive counterflux of $H^+$ and $Ca^{2+}$ bound to these buffers comprises a cytoplasmic $Ca^{2+}/H^+$ exchanger. This acts like a "pump" without a membrane, which can, for instance, recruit $Ca^{2+}$ to acidic cellular microdomains. Cytoplasmic $Ca^{2+}/H^+$

## Significance

**The concentration of $Ca^{2+}$ ions is kept low in cells by specialized ion-pumping proteins at the membrane. We show that in cardiac cells, cytoplasm also has an intrinsic ability to pump $Ca^{2+}$. Histidyl dipeptides and ATP are diffusible cytoplasmic buffer molecules. By exchanging $Ca^{2+}$ for $H^+$, they act like local "pumps," producing uphill $Ca^{2+}$ movement within cytoplasm in response to $H^+$ ion gradients. Intracellular $H^+$ ions are generated locally by metabolism and competitively inhibit many $Ca^{2+}$-activated biochemical processes. Recruiting $Ca^{2+}$ to acidic zones facilitates these processes. Cytoplasmic histidyl dipeptides and ATP thus act like a biological pump without a membrane.**

Author contributions: P.S., K.W.S., and R.D.V.-J. designed research; P.S., J.-B.Y., N.S., and K.W.S. performed research; P.S., J.-B.Y., N.S., C.-H.L., and R.D.V.-J. analyzed data; and P.S. and R.D.V.-J. wrote the paper.

The authors declare no conflict of interest.

This article is a PNAS Direct Submission.

Freely available online through the PNAS open access option.

[1]To whom correspondence should be addressed. E-mail: richard.vaughan-jones@dpag.ox.ac.uk.

This article contains supporting information online at www.pnas.org/lookup/suppl/doi:10.1073/pnas.1222433110/-/DCSupplemental.

exchange adds a spatial paradigm to our understanding of $Ca^{2+}$ and $H^+$ ion signaling.

## Results

**Acidosis Evokes Intracellular $Ca^{2+}$ Release.** Coupling between the cytoplasmic concentrations of $H^+$ and $Ca^{2+}$ ions was first studied in unpaced myocytes superfused with $Na^+$-free/$Ca^{2+}$-free (0Na-0Ca) solutions to block major sarcolemmal routes of $Ca^{2+}$ transport into and out of the cell (including L-type $Ca^{2+}$ channels and NCX). Myocytes were acetoxymethyl (AM)-loaded with cSNARF1 [5-(and-6)-carboxyseminaphtharhodafluor-1] and Indo1 to monitor intracellular pH ($pH_i$) and $[Ca^{2+}]_i$ simultaneously. Whole-cell superfusion with 80 mM acetate acidified the cytoplasm by means of passive entry of acetic acid (Fig. 1 *A*, *i*). This evoked a reversible rise in resting $[Ca^{2+}]_i$ that could be abolished by AM-loading cells with the $Ca^{2+}$ buffer, 1,2-bis(o-aminophenoxy)ethane-N,N,N′,N′-tetraacetic acid (BAPTA; 100 μM). The $[Ca^{2+}]_i$ response (Fig. 1 *A*, *ii*) was delayed relative to the $pH_i$ change, suggesting that the interaction was not an artifact of Indo1 pH-sensitivity.

The $H^+$-evoked $[Ca^{2+}]_i$ rise, in the absence of extracellular $Na^+$ and $Ca^{2+}$, could also be measured with a different $Ca^{2+}$ dye, Fluo3 (Fig. 1 *B*, *i*), whereas use of an AM-loaded $Mg^{2+}$ dye (MagFluo4) in other experiments indicated no simultaneous rise of intracellular $[Mg^{2+}]$ (Fig. 1 *B*, *ii*). The $[Ca^{2+}]_i$ rise was not significantly different in cells superfused with normal $Na^+$ (140 mM) and $Ca^{2+}$ (1 mM) solution ($\Delta F/F_0 = 0.44 \pm 0.05$ or ~50 nM after 1 min; $n = 10$), and it was the same in electrically paced cells (2 Hz; rise in normalized fluorescence $\Delta F/F_0 = 0.43 \pm 0.08$; $n = 7$), suggesting that the net activity of sarcolemmal $Ca^{2+}$ transport over the measured $pH_i$ and $[Ca^{2+}]_i$ range was not sufficient to modify the response. The response was also the same when NHE transporters were blocked with cariporide (30 μM; Fig. 3 *B*, *iii*; $\Delta F/F_0 = 0.46 \pm 0.03$; $n = 17$). However, increasing the driving force for NCX-mediated $Ca^{2+}$ extrusion (by raising extracellular $Na^+$ from 0 to 140 mM at zero extracellular $Ca^{2+}$ in the presence of 30 μM cariporide) altered the $H^+$-evoked response (Fig. 1 *B*, *iv*), indicating that it takes place in a domain accessible to NCX.

Following AM loading, 18 ± 5% ($n = 5$) of cellular Fluo3 fluorescence and 15 ± 10% ($n = 6$) of cellular cSNARF1 fluorescence is attributable to dye partitioning into mitochondria (estimated by surface-membrane permeabilization with 0.005% saponin-containing high $K^+$ buffer, which releases cytoplasmic dye only). To eliminate the possibility that AM-loaded Fluo3 was reporting an $H^+$-evoked $[Ca^{2+}]$ rise in mitochondria, the membrane-impermeant (salt) form of Fluo3 was delivered to the cytoplasm via a cell-attached patch pipette. Acetate exposure evoked a rise in the Fluo3 signal (Fig. 1 *B*, *v*) comparable to that seen with AM-loaded dye (calibration is provided in Fig. S1). Furthermore, pipette loading of the salt form of BAPTA (5 mM) into the cytoplasm abolished the $H^+$-evoked $[Ca^{2+}]_i$ rise (Fig. 1 *B*, *vi*), indicating that the $H^+$-evoked rise in Fluo3 fluorescence is not mitochondrial. Reducing $pH_i$ thus triggers an intracellular release of $Ca^{2+}$ into the cytoplasm.

**$Ca^{2+}$ Is Not Sourced from Organelles.** Experiments were performed to determine the source of the $H^+$-evoked $[Ca^{2+}]_i$ rise. Preincubation of cells with the SERCA inhibitor thapsigargin (10 μM) emptied the SR (10 mM caffeine did not release $Ca^{2+}$) but did not abolish the $H^+$-evoked response (Fig. 1*C*). Thus, SR stores are not the $Ca^{2+}$ source. Indeed, after thapsigargin treatment, a modest increase in the response was observed, possibly because of the inactivation of SERCA as a "$Ca^{2+}$ buffer" (16). Acidic stores (e.g., lysosomes) are not the $Ca^{2+}$ source, because disrupting them with glycyl phenylalanine 2-naphthylamide (100 μM) or bafilomycin (1.5 μM), confirmed to reduce Lysotracker fluorescence by 48 ± 3% ($n = 12$), did not affect the $H^+$-evoked response (Fig. 1*C*), even after several consecutive acetate exposures

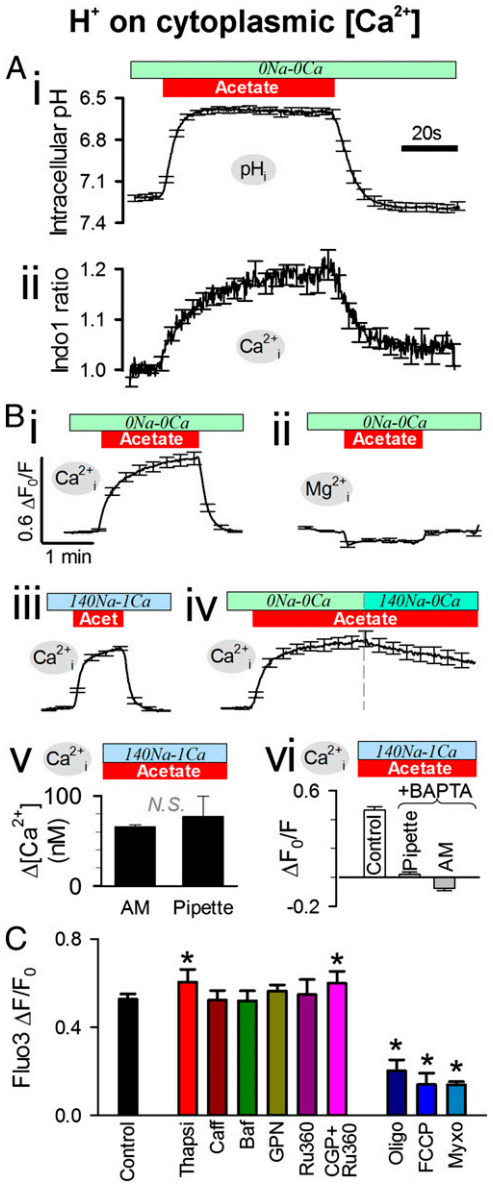


**Fig. 1.** $H^+$ ions evoke intracellular $Ca^{2+}$ release. (*A*) Intracellular pH and $[Ca^{2+}]$ (measured simultaneously with cSNARF1 and Indo1) in rat ventricular myocytes superfused with 0Na-0Ca solution (to eliminate sarcolemmal $Ca^{2+}$ influx and NCX activity). Eighty mM acetate rapidly acidified $pH_i$ and, more slowly, elevated $[Ca^{2+}]_i$ ($n = 10$). (*B*) Acetate (80 mM) in 0Na-0Ca solution evoked a rise in $[Ca^{2+}]_i$ (fluorescence from AM-loaded Fluo3) (*i*) but not in $[Mg^{2+}]$ (MagFluo4) (*ii*). (*iii*) Rise in Fluo3 fluorescence was no different with normal extracellular $Na^+$ and $Ca^{2+}$ (plus 30 μM cariporide to block sarcolemmal NHE). (*iv*) Activating $Ca^{2+}$ extrusion on NCX during acetate exposure evoked a slow $[Ca^{2+}]_i$ recovery (Fluo3). (*v*) Acetate-evoked rise in $[Ca^{2+}]_i$ was no different when Fluo3 salt (100 μM) was pipette-loaded into cells. (*vi*) Rise in $[Ca^{2+}]_i$ (AM-loaded Fluo3) was buffered out by BAPTA (100 μM AM-loaded or 5 mM pipette-loaded) ($n = 5$–30). (*C*) Rise in Fluo3 fluorescence after 2-min exposure to 80 mM acetate in 0Na-0Ca solution. The response was unaffected by 10 mM caffeine (Caff), 1.5 μM bafilomycin (Baf), 100 μM glycyl phenylalanine 2-naphthylamide (GPN), or 10 μM ruthenium-360 (Ru360). The response increased modestly with 10 μM thapsigargin (Thapsi) or 5 μM Ru360 plus 20 μM CGP-37157 (CGP), and it was decreased substantially by metabolic inhibitors: 10 μM oligomycin (Oligo), 1.5 μM FCCP (<15-s exposure), and 10 μM myxothiazol (Myxo) ($n = 15$–30). * denotes significant difference ($P < 0.05$) compared with Control.

(which would have involved cycles of $Ca^{2+}$ release and reuptake). Inhibiting the mitochondrial $Ca^{2+}$ uniporter by preincubation with

ruthenium-360 (Ru360; 10 μM) or blocking mitochondrial NCX with CGP-37157 (20 μM) in the presence of Ru360 (5 μM) also had no effect on the $H^+$-evoked response (Fig. 1*C*), suggesting that mitochondria are not the $Ca^{2+}$ source either. The response, however, was reduced following treatment with the metabolic inhibitors oligomycin A, myxothiazol, and rotenone (all at 10 μM) or FCCP (carbonylcyanide-p-trifluoromethoxyphenylhydrazone, 1 μM for <15 s to avoid excessive cytoplasmic acidification) (Fig. 1*C*). These effects argue that mitochondrial activity may somehow facilitate the $H^+$-evoked response, for example, by supporting metabolism. Hyperpolarization of mitochondrial membrane potential ($\psi_m$) with oligomycin A is opposite to that induced by the other drugs (myxothiazol, rotenone, and FCCP all depolarize), indicating that $\psi_m$ is unlikely to be energizing a mitochondrial $Ca^{2+}$ release (e.g., by driving electrogenic $Ca^{2+}$ flux across the inner mitochondrial membrane). Furthermore, $\psi_m$ (measured with the fluorescent dye JC-1) did not change during cell acidification with acetate (JC-1 ratio was 98 ± 0.03% of control; $n = 6$).

To confirm that mitochondria were not the source for $H^+$-evoked $Ca^{2+}$ release, experiments were performed on saponin-permeabilized myocytes, in which the extramitochondrial environment could be controlled directly by superfusion while recording mitochondrial matrix pH ($pH_m$) or mitochondrial matrix $Ca^{2+}$ ($[Ca^{2+}]_m$) with AM-loaded cSNARF1 or Rhod2, respectively. When permeabilized cells were superfused with an "intracellular" solution at pH 6.6 (i.e., the $pH_i$ in intact cells when superfused with 80 mM acetate), there was a fall in $pH_m$ (Fig. 2*A*), which evoked a rise in $[Ca^{2+}]_m$ (Fig. 2*B*). This $[Ca^{2+}]_m$ rise was still observed when the superfusate was $Ca^{2+}$-free or contained the uniporter blocker, ruthenium red (10 μM) (Fig. 2*C*), suggesting that it may involve $Ca^{2+}$ unloading from mitochondrial matrix buffers. If these $H^+$-mobilized $Ca^{2+}$ ions were then released from the mitochondrion [e.g., via the putative mitochondrial $Ca^{2+}/H^+$ transporter (17)], they would contribute to the $H^+$-evoked rise in cytoplasmic $[Ca^{2+}]$. However, four observations additional to those listed previously (Fig. 1*C*) argue against there being a substantial release. First, the $H^+$-evoked $[Ca^{2+}]_m$ rise did not relax when acid was presented for 5 min (Fig. 2*D*), as would be expected if substantial $Ca^{2+}$ efflux were occurring. Second, in the absence of extramitochondrial $Ca^{2+}$, a repeat exposure to pH 6.6 produced a comparable and reversible $[Ca^{2+}]_m$ response, indicating that total mitochondrial $Ca^{2+}$ had been conserved (Fig. 2*E*), again demonstrating no significant $Ca^{2+}$ efflux. Third, raising extramitochondrial $[Ca^{2+}]$ concurrently with an acid challenge did not significantly enhance the rise of $[Ca^{2+}]_m$ (Fig. 2*F*), as might have been expected if $Ca^{2+}$ efflux were being impeded electrochemically. Fourth, the addition of acid to suspensions of isolated mitochondria raised $[Ca^{2+}]_m$ (measured with Indo1) but did not evoke a substantial rise in extramitochondrial $[Ca^{2+}]$ (measured simultaneously with FuraRed) in a weakly $Ca^{2+}$-buffered solution (containing only 10 μM BAPTA to offset dilution, which would otherwise render $Ca^{2+}$ release unresolvable; Fig. 2 *G*, *i*). This finding argues for little or no $Ca^{2+}$ release. In contrast, FCCP (10 μM) evoked a fall in $[Ca^{2+}]_m$ and a prompt rise in extramitochondrial $[Ca^{2+}]$ (i.e., a positive control for $Ca^{2+}$ release; Fig. 2 *G*, *ii*). In summary, a rise in $[H^+]_i$ can evoke a rise in $[Ca^{2+}]_m$, but this is not the source of $Ca^{2+}$ that underlies cytoplasmic $Ca^{2+}/H^+$ coupling.

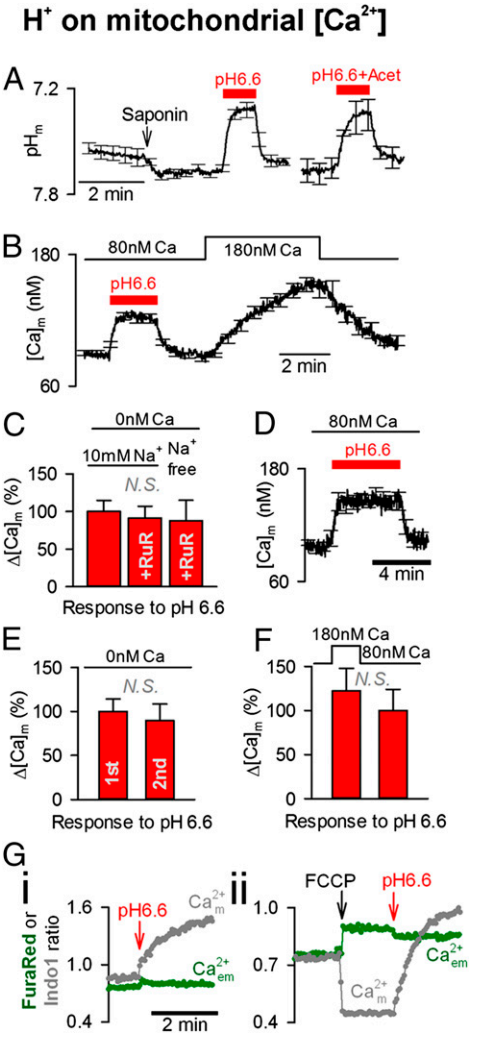


**Fig. 2.** No significant $H^+$-evoked $Ca^{2+}$ release from mitochondria. (*A*) $pH_m$ measured in saponin-permeabilized myocytes AM-loaded with cSNARF1. Exposure to pH 6.6 [with or without 30 mM acetate (Acet)] reduced $pH_m$ ($n$ = 12). (*B*) $[Ca^{2+}]_m$ measured in saponin-permeabilized myocytes AM-loaded with Rhod2. Exposure to pH 6.6 + 30 mM acetate at 80 nM bathing $[Ca^{2+}]$ reversibly raised $[Ca^{2+}]_m$. $H^+$-evoked $[Ca^{2+}]_m$ rise was faster than mitochondrial $Ca^{2+}$ uptake triggered by raising bathing $[Ca^{2+}]$ ($n$ = 15). (*C*) In $Ca^{2+}$-free media, exposure to pH 6.6 in also evoked a rise in $[Ca^{2+}]_m$. Ruthenium red (RuR, 10 μM) did not affect this response ($n$ = 10). (*D*) $[Ca^{2+}]_m$ remained elevated during a long (5-min) exposure to pH 6.6 ($n$ = 8). (*E*) Two consecutive exposures to pH 6.6 in $Ca^{2+}$-free media (7 min apart) evoked comparable $[Ca^{2+}]_m$ responses ($n$ = 6). (*F*) $[Ca^{2+}]_m$ response to pH 6.6 was not significantly larger when bathing $[Ca^{2+}]$ was raised to oppose potential $Ca^{2+}$ efflux ($n$ = 5). (*G*) Suspensions of ventricular mitochondria (1–2 g of protein per liter) in media of low $Ca^{2+}$ buffering power. (*i*) Reducing solution pH from 7.2 to 6.55 raised $[Ca^{2+}]_m$ but did not affect extramitochondrial $[Ca^{2+}]$ ($[Ca^{2+}]_{em}$) measured simultaneously. (*ii*) As a positive control for mitochondrial $Ca^{2+}$ release, FCCP (10 μM) decreased $[Ca^{2+}]_m$ (Indo1) and raised $[Ca^{2+}]_{em}$ (FuraRed). For comparison, brief exposure of thapsigargin-treated intact myocytes to 2 μM FCCP evoked a 69 ± 9% ($n$ = 5) rise in Fluo3 fluorescence.

**$Ca^{2+}/H^+$ Coupling Is Weakened by ATP Depletion.** Cytoplasmic $Ca^{2+}/H^+$ coupling was investigated further by releasing intracellular $H^+$ ions from the photolabile $H^+$ donor compound 2-nitrobenzaldehyde (NBA; 1 mM), permeated passively into intact myocytes from a 0Na-0Ca superfusate (18). A whole-field UV flash rapidly unloads ~1 mM intracellular $H^+$ ions, most of which is buffered. Repeating the UV flash once every 9 s cumulatively induced an intracellular acid load. This is illustrated in Fig. 3 *A*, *i*, where whole-cell $pH_i$ was measured 4.5 s after each flash, at a time when intracellular $H^+$ buffers had reequilibrated. As with acetate superfusion, the intracellular acidosis evoked a rise in cytoplasmic $[Ca^{2+}]$ (measured with Fluo3; Fig. 3 *A*, *i*). The $[Ca^{2+}]_i$ rise was more than that induced by acetate superfusion (compare with Fig. 1*C*), most likely because rapid $H^+$ uncaging by photolysis induces large $pH_i$ transients (Fig. S2) that briefly reach more acidic levels than those recorded after reequilibration (Fig. 3 *A*, *i*). These $[H^+]$ spikes evoke a much greater $Ca^{2+}$ release than possible with slower monotonic increases

in $[H^+]_i$. As with acetate superfusion experiments (Fig. 1*C*), the $H^+$-evoked $[Ca^{2+}]_i$ rise was attenuated by mitochondrial inhibitors (rotenone or antimycin-A), as well as by the glycolytic inhibitor, deoxyglucose (DOG), shown by the left and downward shifts in the pH/$Ca^{2+}$ relationships (Fig. 3 *A*, *ii*). The results suggest that the $H^+$-evoked $[Ca^{2+}]_i$ rise is facilitated by glycolysis and mitochondrial respiration. The degree of inhibition was proportional to the reduction in intracellular ATP ($ATP_i$) (Fig. 3 *A*, *iii*; measured with a luciferin-luciferase assay). The largest inhibition was obtained with a combination of DOG and antimycin, which also produced the largest depletion of $ATP_i$. Metabolic stress, resulting in $ATP_i$ depletion, thus attenuates cytoplasmic $Ca^{2+}/H^+$ coupling.

**Competitive $Ca^{2+}/H^+$ Binding Underlies $Ca^{2+}/H^+$ Coupling.** When the area of photolytic $H^+$ uncaging was restricted to a central 5 × 5-μm region of the myocyte, the local $H^+$ load (Fig. 3 *B*, *i*) evoked a local $[Ca^{2+}]_i$ rise (Fig. 3 *B*, *ii*) that, again, could be buffered out by BAPTA (AM-loaded, 100 μM; Fig. 3 *B*, *iii*). After local release, the diffusive spread of $Ca^{2+}$ was slower than for $H^+$ ions, as expected from their cytoplasmic diffusion coefficients (10, 18, 19) and in agreement with a cytoplasmic site for $Ca^{2+}$ release. Moreover, thapsigargin (10 μM) accelerated $Ca^{2+}$ mobility (Fig. 3 *B*, *iv*), as expected from the inability of blocked SERCA pumps to restrict $Ca^{2+}$ diffusion. Also in agreement with the previous findings, the $[Ca^{2+}]_i$ response was substantially reduced in the presence of the mitochondrial inhibitor myxothiazol (Fig. 3 *B*, *v*). Thus, $H^+$-induced $Ca^{2+}$ release can be evoked both globally and locally within the cytoplasmic compartment, it is metabolically sensitive, and it is not due to $Ca^{2+}$ release from organelles. Cytoplasmic $Ca^{2+}/H^+$ coupling thus appears to be an intrinsic property of cytoplasm caused by the ion-binding characteristics of its constituent buffers.

To test the possibility that $Ca^{2+}/H^+$ coupling is due to cytoplasmic buffers, a panel of candidate buffers was screened in vitro for $Ca^{2+}$ unloading upon $H^+$ uncaging. Hemoglobin (Hb), which is rich in $H^+$-binding histidine residues, was chosen to represent a poorly mobile cytoplasmic protein buffer [1 mM Hb matches the intrinsic $H^+$ buffering capacity typically measured in myocytes (4)]. Carnosine (a dipeptide composed of β-alanine and histidine) was selected to represent the group of cytoplasmic histidyl dipeptide (HDP) buffers. These comprise carnosine, anserine (β-alanine-methylhistidine) and homocarnosine (GABA-histidine), and they are collectively present in ventricular myocytes at ~17 mM [based on biochemical analyses (11, 20, 21) and measurements of mobile $H^+$ buffering capacity (11, 22, 23)]. Individual buffers were mixed with NBA (5 mM) in solutions containing Hepes and BAPTA and the salt form of either cSNARF1 or FuraRed to measure pH or $Ca^{2+}$, respectively (Fig. 3). To reduce convective movement, solutions were mixed with low-melting-point agarose, heated to 70 °C, aliquoted in 100-μL volumes onto glass coverslips, and allowed to set. UV uncaging of $H^+$ ions into these agarose gels evoked significant unloading of $Ca^{2+}$ from Hb, carnosine, and ATP (Fig. 3 *C*, *i*). These buffer types are thus likely to contribute to cytoplasmic $Ca^{2+}/H^+$ coupling. Importantly, much smaller amounts of $Ca^{2+}$ were unloaded from ADP or inorganic phosphate ($P_i$), which may explain the reduction in $H^+$-evoked $Ca^{2+}$

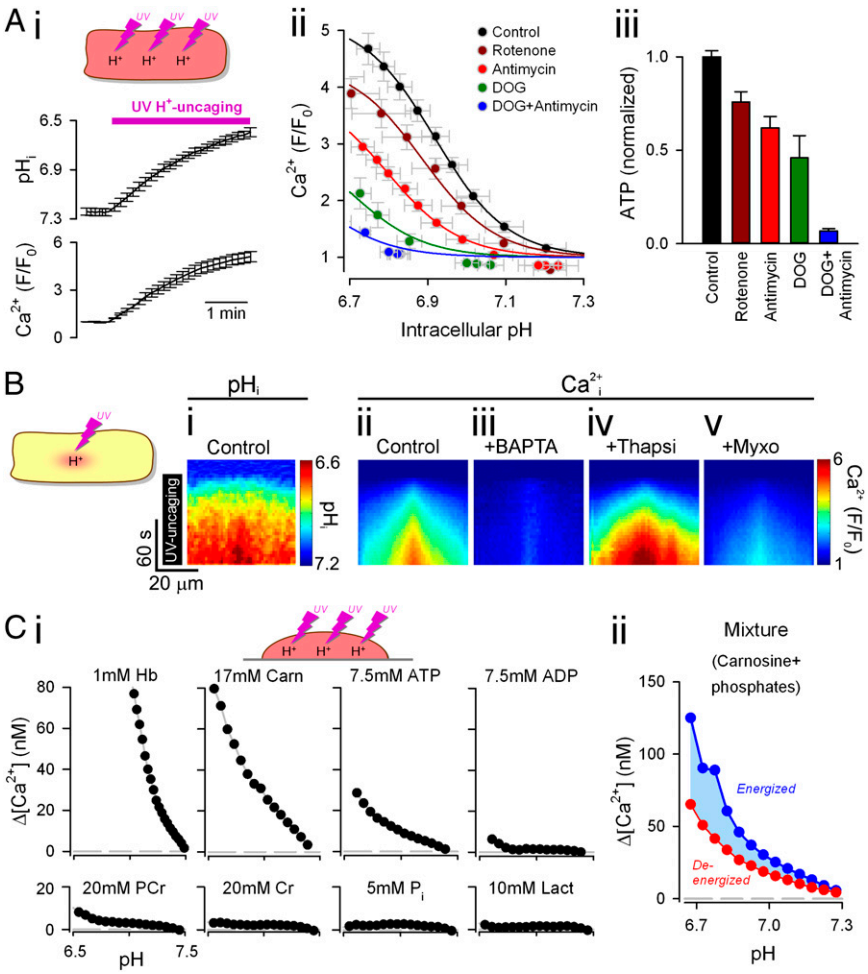


**Fig. 3.** $H^+$-evoked unloading of $Ca^{2+}$ from cytoplasmic buffers depends on the metabolic state. (*A*) $H^+$ uncaging by whole-field UV flash every 9 s in rat ventricular myocytes passively loaded with photolabile $H^+$ donor NBA (1 mM) dissolved in 0Na-0Ca superfusate. (*i*) Intracellular pH (cSNARF1) and $[Ca^{2+}]$ (Fluo3) were measured after each flash ($n$ = 35). (*ii*) $pH_i$-$[Ca^{2+}]_i$ relationship was highly sensitive to metabolic inhibition. Deoxyglucose (DOG; 5 mM) and all other drugs (10 μM) were added 3 min before the onset of $H^+$ uncaging. (*iii*) ATP content in populations of isolated myocytes was assayed (luciferase bioluminescence) 20 min after exposure to drugs. Luminescence was calibrated using an ATP standard, divided by the number of myocytes staining positively for trypan blue (i.e., living cells), and subsequently normalized to the measurement under control conditions ($n$ = 3). (*B*) Confocal line scans. UV flash ($H^+$ uncaging) was confined to a central 5 × 5-μm region of intact myocytes. Lateral diffusive spread of $[H^+]$ (*i*) and $[Ca^{2+}]$ (*ii*). (*iii*) $[Ca^{2+}]$ response was abolished by BAPTA (100 μM AM-loaded). (*iv*) Diffusive spread was accelerated with thapsigargin (Thapsi; 10 μM). (*v*) $[Ca^{2+}]$ response was reduced in myxothiazol (Myxo; 10 μM). (*C*) (*i*) Uncaging of $H^+$ ions in vitro in agarose-set mixtures of buffers (plus Hepes and BAPTA to adjust initial pH to 7.4 and $[Ca^{2+}]_i$ to 60 nM). Hb, haemoglobin; Carn, carnosine; PCr, phosphocreatine; Cr, creatine; Pi, inorganic phosphate; Lact, lactate. (*ii*) Mixture of carnosine (Carn) and phosphates, representing a fully energized state (7.5 mM ATP, 20 mM PCr) or a fully deenergized state (7.5 mM ADP, 20 mM Cr, 27.5 mM $P_i$). Starting pH, $[Mg^{2+}]$ and $[Ca^{2+}]_i$ were adjusted to 7.2, 0.75 mM and 100 nM, respectively.

release observed after metabolic inhibition, when intracellular ATP levels fall and ADP and $P_i$ levels rise. This explanation was tested further by uncaging $H^+$ into gels containing mixtures of carnosine (17 mM) plus phosphates representing a fully energized cytoplasmic compartment [7.5 mM ATP, 20 mM phosphocreatine (PCr)] or a deenergized compartment [7.5 mM ADP, 20 mM creatine (Cr), 27.5 mM $P_i$] at 100 nM [$Ca^{2+}$] and 0.75 mM [$Mg^{2+}$]. Results show that the $Ca^{2+}$ yield per uncaged $H^+$ was reduced by ~40% when all ATP and PCr were dephosphorylated (Fig. 3 *C*, *ii*). This situation is equivalent to full metabolic inhibition, suggesting that metabolic stress may attenuate cytoplasmic $Ca^{2+}$/$H^+$ coupling in the intact myocyte, by reducing $[ATP]_i$, and hence the availability of common $Ca^{2+}$/$H^+$ buffer sites. The reduced coupling in vitro (40%; Fig. 3 *C*, *ii*), however, was smaller than obtained in metabolically inhibited myocytes (>90%; Fig. A, *ii*), implying that additional factors, such as the rise of intracellular [$Mg^{2+}$] ($[Mg^{2+}]_i$), known to be associated with $[ATP]_i$ depletion, may also play a role in intact cells.

**$H^+$-Evoked [$Ca^{2+}$] Microdomain That Does Not Dissipate.** The spatial interaction between $H^+$ and $Ca^{2+}$ ions was probed by imaging $[Ca^{2+}]_i$ in an intact myocyte while imposing a standing cytoplasmic $[H^+]_i$ gradient induced by continuous exposure of one end of the cell to acetate. The maneuver was performed using a dual-microperfusion device that releases two parallel streams of solution (acetate-containing and acetate-free 0Na-0Ca) oriented perpendicular to a myocyte (14). Sustained entry of acetic acid into the exposed end of the cell, balanced by its exit at the opposite end, generates a $pH_i$ gradient of up to 0.6 $pH_i$ units (Fig. 4 *A*, *i*; imaged after 5 min of dual microperfusion). The magnitude of this gradient depended on the position of the microstream boundary across the cell (Fig. 4 *B*, *i*) and remained stable for as long as local acetate exposure was maintained (Fig. 4 *C*, *i*). In Fluo3-loaded myocytes, imposing the longitudinal $pH_i$ gradient generated a local $[Ca^{2+}]_i$ rise in the acidified region of the cell (Fig. 4 *A*, *ii*; an end-to-end $[Ca^{2+}]_i$ gradient of ~80 nM). Resting $[Ca^{2+}]_i$ thus mapped spatially onto the $pH_i$ gradient (Fig. 4*B*).

Local $H^+$-evoked unloading of $Ca^{2+}$ from buffers will release $Ca^{2+}$ that should then diffuse away. In this model, the local $[Ca^{2+}]_i$ gradient should dissipate within a minute or so. However, the observed end-to-end $[Ca^{2+}]_i$ gradient was sustained, and actually increased in amplitude over a period of several minutes (Fig. 4 *C*, *ii*), even though the $pH_i$ gradient remained constant (Fig. 4 *C*, *i*), suggesting that $Ca^{2+}$ was being transported uphill into the acidic zone at a rate that exceeded its dissipative flux in the opposite direction. A sustained acid microdomain within the cytoplasmic compartment of a ventricular myocyte thus induces a sustained $Ca^{2+}$ microdomain. The [$Ca^{2+}$] gradient was abolished in 100 μM BAPTA-AM–loaded cells (Fig. S3*A*) but was unaffected by maneuvers that alter sarcolemmal $Ca^{2+}$ flux, suggesting it was maintained via an intracellular mechanism. Such maneuvers included raising microstream [$Na^+$] from zero to 140 mM (Fig. S3*B*), with or without a concurrent 1 mM rise in microstream

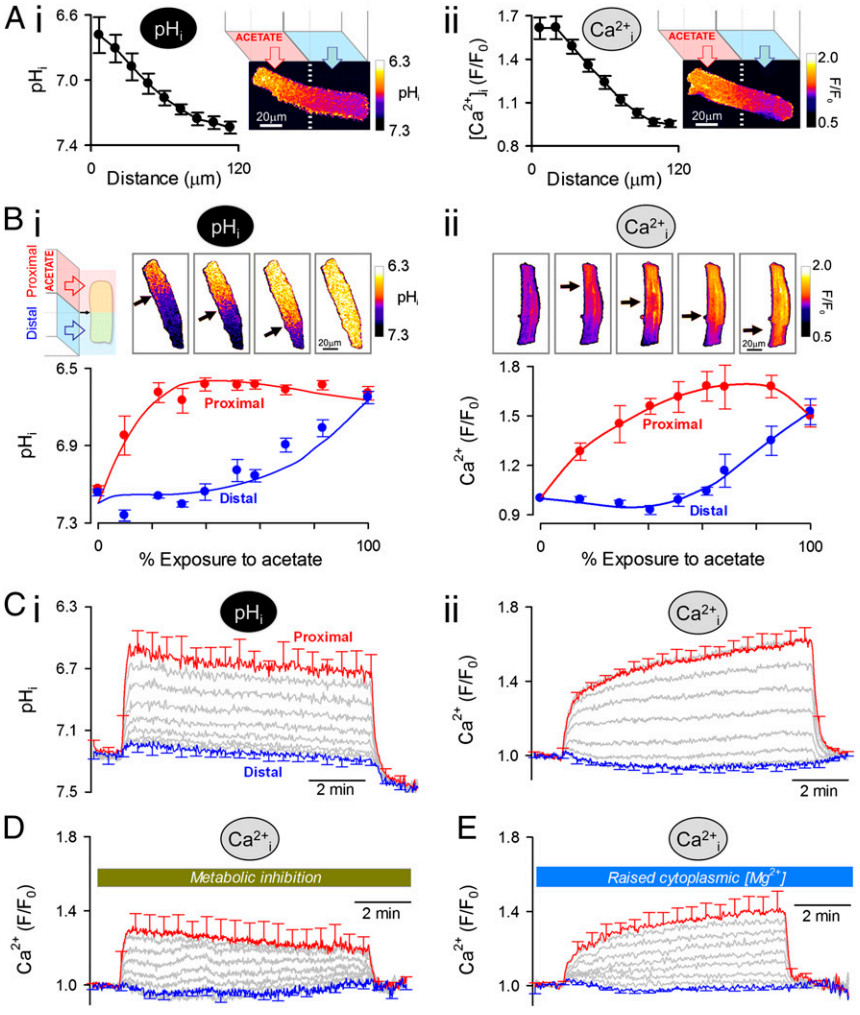


**Fig. 4.** Stable, spatial $[H^+]_i$ gradient induces a standing $[Ca^{2+}]_i$ gradient. (*A*) 0Na-0Ca superfusates. A standing $pH_i$ gradient (cSNARF1) (*i*) and a $Ca^{2+}$ gradient (Fluo3; measured in a separate experiment) (*ii*) were generated by regional exposure of a myocyte using a dual-microperfusion apparatus (80 mM acetate in proximal microstream). Red and blue arrows show flow direction ($n$ = 15 and $n$ = 18). (*B*) $pH_i$ (*i*) and $Ca^{2+}$ (*ii*), measured separately, plotted for different degrees of acetate exposure and measured after 5 min of dual microperfusion in two regions of the myocyte. The size of regions was the cell width × one-ninth of the cell length ($n$ = 10–20 per bin). The black arrow indicates the position of the microstream boundary. (*C*) Time-course of *(i)* $pH_i$ and *(ii)* $[Ca^{2+}]_i$ (measured separately) averaged in nine adjacent regions aligned along the length of the myocyte ($n$ = 20). (*D*) Time course of $[Ca^{2+}]_i$ measured under metabolic inhibition (10 μM rotenone, 10 μM antimycin A, 5 mM deoxyglucose) ($n$ = 15). (*E*) Time course of $[Ca^{2+}]_i$ measured in myocytes loaded with fourfold raised $[Mg^{2+}]_i$ (exposure to 0Na, 30 mM $Mg^{2+}$ containing superfusate) ($n$ = 10).

$[Ca^{2+}]$ (Fig. S3*C*), or electrically pacing cells at 2 Hz in buffer containing 140 mM $Na^+$ and 1 mM $Ca^{2+}$ (Fig. S3*D*). The plasmalemmal $Ca^{2+}/H^+$ ATPase pump (PMCA), which potentially remained functional under all the above experimental conditions, could conceivably have coupled intracellular microdomains of $[H^+]$ and $[Ca^{2+}]$, but this requires sarcolemmal $Ca^{2+}$ influx to raise $[Ca^{2+}]_i$ locally in the acid microdomain. Given that $[Ca^{2+}]_i$ gradients were readily measured in the absence of extracellular $Ca^{2+}$, this mechanism is unlikely. Nevertheless, although PMCA did not cause the $[Ca^{2+}]_i$ gradient, neither did it prevent the sustained $[Ca^{2+}]_i$ rise in acidic zones, suggesting that its activity was downregulated by the fall of $pH_i$ (24). Indeed this appears to have been the case, as inhibiting PMCA further (achieved by raising extracellular $[Ca^{2+}]$ to 8 mM) increased $[Ca^{2+}]_i$ gradients only modestly (Fig. S3*E*). The involvement of the SR or mitochondria in maintaining the $[Ca^{2+}]_i$ gradient was tested pharmacologically. Thapsigargin (10 μM) or the combination of CGP-37157 (20 μM) plus Ru360 (5 μM) did not collapse the $Ca^{2+}$ microdomain (Fig. S3*F*), suggesting that uphill $Ca^{2+}$ delivery to the acidic domain was neither SR- nor mitochondrion-dependent. Uphill $Ca^{2+}$ transport into the acidic microdomain (i.e., $Ca^{2+}$ flux up the spatial $[H^+]_i$ gradient) must have involved endogenous cytoplasmic molecules.

Cytoplasmic $H^+$ ion mobility is mediated through reversible $H^+$ binding to small diffusible buffers, such as HDPs (11, 25). The imposition of a stable $[H^+]_i$ gradient using dual microperfusion will therefore result in a large and continuous diffusive flux of unprotonated mobile buffer molecules into the acidic region, where they will be loaded with $H^+$ ions. If an unprotonated molecule were able reversibly to bind $Ca^{2+}$ ions more readily than the protonated molecule, $[Ca^{2+}]_i$ would build up in the acidic zone (Fig. S4). In effect, $H^+$ ions would displace $Ca^{2+}$ from the incoming buffer. Buffer molecules that had discharged $Ca^{2+}$ and acquired $H^+$ ions would then diffuse to more alkaline regions of the cell, where the reverse process would occur (i.e., discharge of $H^+$ ions in exchange for $Ca^{2+}$ binding). The flux of $Ca^{2+}$-loaded buffer into the acidic microdomain would thus be maintained indefinitely, allowing a local elevation of $Ca^{2+}$ that did not dissipate spatially. On the basis of their low molecular weight and pH-sensitive $Ca^{2+}$-binding properties (Fig. 3*C*), HDPs and ATP could mediate this $Ca^{2+}/H^+$ exchange. Performing dual microperfusion during metabolic inhibition of a myocyte (with a combination of rotenone, antimycin, and DOG) did not affect the size of the imposed $[H^+]_i$ gradient [0.52 ± 0.05 $pH_i$ units ($n$ = 5) vs. 0.56 ± 0.04 control; Fig. S5*A*], but it collapsed the end-to-end $[Ca^{2+}]_i$ gradient by ∼60% (Fig. 4*D*). Metabolic inhibition did not affect total cellular HDP content (in vitro assay of lysates of control and DOG-treated hearts: 1.09 ± 0.12 and 1.04 ± 0.15 mM HDPs per gram of protein, respectively) (25), but it reduced $[ATP]_i$ by up to 95% (Fig. 3 *A*, *iii*). Collapse of the $H^+$-induced $[Ca^{2+}]_i$ gradient may result from the depletion of diffusible ATP molecules, or from a reduction in the $Ca^{2+}$-carrying capacity of diffusible HDPs.

To test the effect of reducing the $Ca^{2+}$-binding capacity of HDPs, advantage was taken of their similar affinity for $Ca^{2+}$ and $Mg^{2+}$. This feature is not evident among other intracellular $Ca^{2+}$ buffer molecules, such as troponin or calmodulin. Because the $Mg^{2+}$ affinity of HDPs is ∼0.7 mM (26), any rise in $[Mg^{2+}]_i$ from its resting level of 0.75 mM will decrease HDP $Ca^{2+}$ occupancy. Myocytes (in $Ca^{2+}$-free media) were $Mg^{2+}$-loaded by raising extracellular $[Mg^{2+}]$ from 1 to 30 mM and removing extracellular $Na^+$ (27). This maneuver increased MagFluo4 fluorescence fourfold with a time constant of 3 min (Fig. S5*B*), without changing $pH_i$ or greatly altering $[Ca^{2+}]_i$ (which increased by ∼10%). Applying dual microperfusion to a myocyte with raised $[Mg^{2+}]_i$ did not change the imposed $pH_i$ gradient (0.53 ± 0.1 pH units; $n$ = 4), but it reduced the overlying end-to-end $[Ca^{2+}]_i$ gradient by ∼40% (Fig. 4*E*), suggesting that when the $Ca^{2+}$-carrying capacity of HDPs is compromised, so is the uphill recruitment of $Ca^{2+}$ to an acidic microdomain. The observation provides evidence for the participation of HDPs in sustaining a $Ca^{2+}$ microdomain. Metabolic inhibition is known to raise $[Mg^{2+}]_i$ and deplete $ATP_i$ (by liberating $Mg^{2+}$ during net MgATP hydrolysis); thus, these changes now provide a mechanism for the attenuation of the $Ca^{2+}$ microdomain by metabolic inhibitors (Fig. 4*D*), through reduction of available mobile $Ca^{2+}/H^+$-binding sites.

**Testing the Cytoplasmic $Ca^{2+}/H^+$ Exchange Hypothesis.** The cytoplasmic $Ca^{2+}/H^+$ exchange hypothesis was tested further with three experimental maneuvers that did not involve regional acetate exposure. In the first maneuver, a stable $[H^+]_i$ gradient was generated in a myocyte by stimulating sarcolemmal acid/base transporters. Using dual microperfusion (Fig. 5 *A*, *i*), net acid extrusion via NHE was stimulated at one end of the cell (with a $Cl^-$-free superfusate of high pH) and net acid influx via CHE was stimulated at the other end (with a $Na^+$-free superfusate of low pH). This maneuver resulted in a stable, end-to-end $[H^+]_i$ gradient of 0.14 $pH_i$ units (Fig. 5 *A*, *ii*). The $[H^+]_i$ gradient then induced a stable $[Ca^{2+}]_i$ gradient of 0.2 $F/F_0$ units (∼25 nM $Ca^{2+}$; Fig. 5 *A*, *iii*). Thus, as with local acetate exposure, cytoplasmic $[Ca^{2+}]$ maps stably onto a transporter-induced $pH_i$ gradient.

A second maneuver was used to investigate whether cytoplasmic $Ca^{2+}/H^+$ exchange could work in reverse and generate an $[H^+]_i$ gradient in response to an experimentally imposed cytoplasmic $[Ca^{2+}]$ gradient (Fig. 5 *B*, *i*). Dual microperfusion delivered $Na^+$-free solution containing 100 μM $Ca^{2+}$ to one end of the cell (stimulating net $Ca^{2+}$ influx by NCX) and $Ca^{2+}$-free solution containing 140 mM $Na^+$ to the other end (stimulating net $Ca^{2+}$ efflux by NCX). This led, in the steady state, to a large longitudinal $[Ca^{2+}]_i$ gradient of ∼7 $F/F_0$ units (equivalent to ∼5 μM $Ca^{2+}$; Fig. 5 *B*, *ii*), which, in turn, led to an end-to-end $pH_i$ gradient of 0.2 units (Fig. 5 *B*, *iii*). Thus, under appropriate conditions, $pH_i$ maps stably onto a transporter-induced $[Ca^{2+}]_i$ gradient.

Given that global metabolic inhibition collapses an $H^+$-evoked $Ca^{2+}$ microdomain (Fig. 4*D*), a third maneuver was devised to test if a spatially localized metabolic microdomain could induce microdomains for $[Ca^{2+}]$ and $[H^+]$. Using dual microperfusion, one-half of a myocyte was exposed to FCCP (0.5 μM) to trigger net ATP hydrolysis locally and drive the reverse reaction at the opposite end of the cell. ATP diffusion into the FCCP-treated end, in exchange for ADP, completes the cycle. This experimental maneuver produced stable overlying gradients of $[H^+]_i$ and $[Ca^{2+}]_i$ (Fig. 5*C*). The $[H^+]_i$ gradient may be explained by $H^+$ release during ATP hydrolysis at one end of the cell and $H^+$ consumption by the reverse reaction at the other. The $[Ca^{2+}]$ gradient is explained by two processes. First, diffusion of CaATP (and MgATP) will deliver $Ca^{2+}$ (and $Mg^{2+}$) to the metabolically inhibited end of the cell, whereupon ATP is hydrolyzed and the divalent cations are released. Second, the local elevation of $[H^+]_i$ and $[Mg^{2+}]_i$ resulting from ATP hydrolysis will cause $H^+$-loaded and $Mg^{2+}$-loaded HDPs to diffuse out toward the metabolically functional end of the cell, in exchange for $Ca^{2+}$-bound buffer. Thus, a localized zone of metabolic stress is signified by a localized and sustained rise of both $[Ca^{2+}]_i$ and $[H^+]_i$.

Therefore, three very different experimental maneuvers support predictions of a mobile cytoplasmic $Ca^{2+}/H^+$ exchange.

## Discussion

The present work establishes that the spatial homogeneity of resting (diastolic) $Ca^{2+}$ in ventricular myocytes is labile, being readily disturbed by changes in $[H^+]_i$. Both local and global elevations of cytoplasmic $[H^+]_i$ increase cytoplasmic $[Ca^{2+}]_i$, but the surprising observation is that when localized acidosis is sustained, it produces an equally localized and sustained rise of $[Ca^{2+}]_i$ that does not dissipate spatially. Although this latter

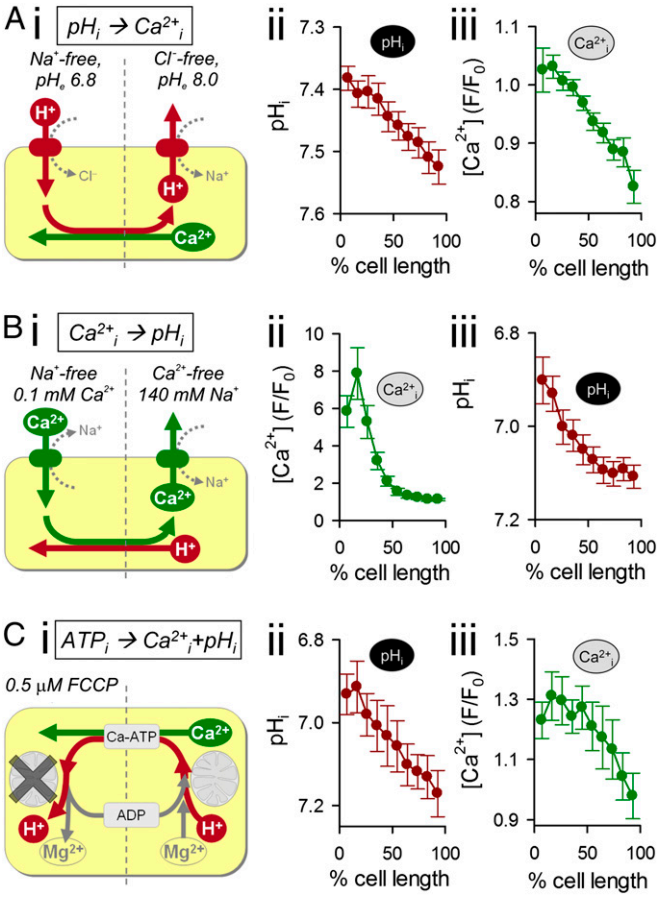


**Fig. 5.** Testing the cytoplasmic $Ca^{2+}/H^+$ exchanger hypothesis. (*A*) Longitudinal, standing $[H^+]$ gradient established by activating acid influx on $Cl^-/OH^-$ exchange and acid efflux on $Na^+/H^+$ exchange, at opposite ends of the myocyte, using dual microperfusion. The $[H^+]_i$ gradient produces a standing $[Ca^{2+}]$ gradient (measured in separate experiments; $n = 12$). (*B*) Longitudinal, standing $[Ca^{2+}]$ gradient established by activating $Na^+/Ca^{2+}$ exchange in inward and outward modes at opposite ends of cell using dual microperfusion. The $[Ca^{2+}]_i$ gradient produces a standing $[H^+]_i$ gradient (measured in separate experiments; $n = 8$). (*C*) Metabolic inhibition confined to one end of the cell produces a local, sustained rise in $[H^+]_i$ and $[Mg^{2+}]_i$, which then drives longitudinal ATP/ADP exchange in the cytoplasm. This generates a localized rise of $[Ca^{2+}]_i$ in the metabolically challenged end of the cell ($pH_i$ and $[Ca^{2+}]_i$ measured separately; $n = 7$).

reaction requires the uphill transport of $Ca^{2+}$ ions, it is an intrinsic property of cytoplasm. Local $pH_i$ nonuniformity is known to occur within cells, as discussed elsewhere in this paper; thus, spatial $Ca^{2+}/H^+$ interaction is likely to be a frequent event. The coupling is not dependent on $Ca^{2+}$ movement at organelles like the SR, acidic stores, or mitochondria. It occurs within seconds; as a result, cytoplasmic $Ca^{2+}$ in the myocyte maps spatially onto $pH_i$. The reaction is physiologically relevant because nanomolar displacements of $[H^+]_i$ (equivalent to fractions of a $pH_i$ unit) lead to nanomolar changes in $[Ca^{2+}]_i$. The $H^+$-evoked rise of $[Ca^{2+}]_i$ is caused by these ions sharing common intracellular buffer sites on proteins and other molecules. However, the ability of $Ca^{2+}$ to map stably onto spatially varied $[H^+]_i$ is dependent on a subclass of small molecules that display competitive $Ca^{2+}/H^+$ binding but are also diffusible. Notable among these are HDPs and ATP. By exchanging $Ca^{2+}$ for $H^+$, these molecules act like local pumps within cytoplasm, producing spatial uphill $Ca^{2+}$ transport in response to local $[H^+]_i$ gradients. We evaluate here the cytoplasmic source of $Ca^{2+}/H^+$ coupling, its spatial properties, and its physiological significance.

**Cytoplasmic Buffers Underlie Cytoplasmic $Ca^{2+}/H^+$ Coupling.** Resting $[Ca^{2+}]_i$ (normally ~100 nM) sets the background level of $Ca^{2+}$ signaling in a cell and determines the threshold for triggering more elaborate spatiotemporal patterns of signaling. In the present work, we have shown that reducing resting $pH_i$ by about 0.6 units using acetate superfusion (equivalent to an $[H^+]_i$ elevation of 190 nM; Fig. 1*A*), raises resting $[Ca^{2+}]_i$ by about 60 nM (Fig. 1*C*). Both $Ca^{2+}$ release from mitochondria and functional coupling between sarcolemmal NHE and NCX transporter activities have previously been postulated as important underlying mechanisms (9, 28). We find, however, that although a rise of mitochondrial matrix $[Ca^{2+}]$ occurs in response to low cytoplasmic pH, significant $Ca^{2+}$ efflux does not ensue (Fig. 2). Similarly, $Ca^{2+}$ release from the SR or acidic stores, or $[Ca^{2+}]_i$ elevation via sarcolemmal NHE/NCX coupling, has also been excluded, although the latter mechanism is known to enhance electrically evoked $Ca^{2+}$ transients during acidosis (7, 8). Instead, diastolic $Ca^{2+}/H^+$ coupling in the ventricular myocyte relies on buffer molecules with $H^+$-sensitive $Ca^{2+}$ affinity. As a result, diastolic $Ca^{2+}$ and $H^+$ levels rise and fall in tandem. This coupling (9, 29, 30) was first mooted more than 30 y ago, but with no evidence for the nature or identity of the $Ca^{2+}/H^+$-binding sites. We now show that $Ca^{2+}$ unloading from histidyl molecules is likely to be a key component. Histidine residues are sited on many proteins within the cytoplasmic compartment, including known $Ca^{2+}$ buffers like troponin, calmodulin, and SERCA, as well as the smaller, more readily diffusible HDP molecules like carnosine, anserine, and homocarnosine (~250 Da). In addition, we have demonstrated ATP to be an important $H^+$-releasable source of $Ca^{2+}$ (31) (Fig. 3*C*). $Ca^{2+}$ release from proteins and HDPs may involve binding of $H^+$ and $Ca^{2+}$ ions to common sites (e.g., at imidazole groups), or it may involve a more sophisticated intramolecular reorganization of the buffer molecule that changes binding affinities.

The effective $Ca^{2+}$ affinity of HDPs is modulated by $Mg^{2+}$ as well as $H^+$ ions. A rise in $[Mg^{2+}]_i$ will displace $Ca^{2+}$ because, unusually among cytoplasmic mobile $Ca^{2+}$ buffers, both ions have similar binding affinities. Displacement will then reduce the functional expression of cytoplasmic $Ca^{2+}/H^+$ coupling in a manner analogous to the effects of competitive inhibitors on membrane transporter proteins. Metabolic inhibition also reduces the $H^+$-sensitivity of diastolic $[Ca^{2+}]$ (Fig. 3 *A*, *ii*), an effect caused partly by the fall in $[ATP]_i$ (which reduces the availability of $Ca^{2+}/H^+$-binding sites) and partly by the rise of $[Mg^{2+}]_i$ under these conditions (which reduces $Ca^{2+}$ binding by HDPs). Thus, cytoplasmic $Ca^{2+}/H^+$ coupling exhibits plasticity through its sensitivity to the cell's energetic status.

**Cytoplasmic $Ca^{2+}/H^+$ Exchange: A Pump Without a Membrane.** The present work has demonstrated that a spatial cytoplasmic $[Ca^{2+}]$ microdomain maps automatically onto an $H^+$ microdomain, and vice versa. Although the $H^+$-evoked $Ca^{2+}$ response occurs within seconds, the spatially confined $Ca^{2+}$ microdomain is sustained for the lifetime of the $H^+$ microdomain (tested here for several minutes). Theoretically, an 80-nM longitudinal $[Ca^{2+}]_i$ gradient, such as that observed during dual microperfusion (Fig. 4 *A*, *ii*), could be generated by sarcolemmal $Ca^{2+}$ influx (at 10 μM/min) into the acidic end of the cell, coupled with an equal $Ca^{2+}$ efflux from the nonacidic end. However, because the same $[Ca^{2+}]$ nonuniformity is observed under different bathing conditions (varying extracellular $[Na^+]$ and $[Ca^{2+}]$; Fig. S3), such a sarcolemmal flux arrangement is highly unlikely, particularly because the $[Ca^{2+}]_i$ gradient persists in $Ca^{2+}$-free media. Instead, spatial $Ca^{2+}/H^+$ coupling must involve a cytoplasmic mechanism. This requires cytoplasmic $Ca^{2+}/H^+$ buffer molecules of adequate mobility (i.e., of low molecular weight). The $[H^+]_i$ gradient drives a diffusive flux of protonated buffer out of the acidic region, and a counterflux of unprotonated buffer (Fig. 6*A*). Due to compet-

itive $Ca^{2+}/H^+$ binding, the counterflux delivers $Ca^{2+}$ to the acidic microdomain, thus offsetting the tendency for $Ca^{2+}$ to diffuse away. For the process to occur optimally, the concentrations of protonated and unprotonated buffer must be similar (i.e., the mobile buffer's acid dissociation constant $pK_H$ must be in the physiological pH range) and the $Ca^{2+}$ affinity of the unprotonated buffer must be sufficient to carry a significant $Ca^{2+}$ cargo. All these conditions are satisfied for cytoplasmic HDPs (26), which spatially traffic most of the diffusive $H^+$ flux within the cell (11, 14, 25), and for ATP. Although Fluo3 is technically a $Ca^{2+}/H^+$ buffer (32), it is not capable of generating the observed $Ca^{2+}$ gradients because of its low cytoplasmic concentration, low intracellular diffusion coefficient (19), and low $H^+$ affinity (32) (*Mathematical Supplement*). The uphill recruitment of $Ca^{2+}$ ions via HDP and ATP molecules to an acidic microdomain is thus coupled to a downhill counterflux of $H^+$ ions via the same buffers. Provided the spatial gradient for $H^+$ ions is maintained by some other source, so is the uphill recruitment of $Ca^{2+}$, financed thermodynamically by the energy stored in the spatial $[H^+]_i$ gradient. The phenomenon is therefore an example of a simple $Ca^{2+}/H^+$ exchange ion transporter, operating spatially within the cytoplasmic compartment. The diffusible $Ca^{2+}/H^+$ carriers act like a pump without a membrane (Fig. 6*A*).

The formalism more generally used to describe the kinetics of membrane transport can also be applied to cytoplasmic $Ca^{2+}/H^+$ exchange. $V_{max}$ can be approximated from the mobile buffer's concentration ($C$), diffusion coefficient ($D$), and distance ($l$) as $1/2 \times C \times D/l^2$. At resting cytoplasmic pH and $Ca^{2+}$ levels, the $H^+$:$Ca^{2+}$ stoichiometry ($S_{H:Ca}$) is ~2,400:1 for HDPs and ~40:1 for ATP (derived from the buffer's $H^+$ and $Ca^{2+}$ occupancy). The size of $[Ca^{2+}]$ nonuniformity ($\Delta[Ca^{2+}]$) can be predicted from the $[H^+]$ gradient ($\Delta[H^+]$) using an approximation featuring $S_{H:Ca}$, $H^+$, and $Ca^{2+}$ buffering ratio ($\beta_H$ ~ 1:200,000; $\beta_{Ca}$ ~ 1:200), as well as a variable ($\alpha_H$ or $\alpha_{Ca}$) that describes the fraction of $H^+$ or $Ca^{2+}$ flux carried by mobile $Ca^{2+}/H^+$ buffer (as opposed to noncompetitively binding mobile buffers):

$$\Delta[Ca^{2+}] = \alpha_H \times \Delta[H^+] \times \beta_{Ca}/(S_{H:Ca} \times \beta_H), \quad [1]$$

$$\Delta[H^+] = \alpha_{Ca} \times \Delta[Ca^{2+}] \times (S_{H:Ca} \times \beta_H)/\beta_{Ca}. \quad [2]$$

Thus, a rise in $[Mg^{2+}]_i$, by increasing $S_{H:Ca}$, reduces $[H^+]$-evoked $[Ca^{2+}]$ gradients (Fig. 4*D*). In response to an $[H^+]$ gradient, HDPs can produce a large $[Ca^{2+}]$ gradient because the majority of diffusive $H^+$ flux is carried by these buffers (i.e., $\alpha_H$ close to 1). Although ATP is a minor $H^+$ buffer, it contributes toward $[Ca^{2+}]$ gradient formation because of its lower $S_{H:Ca}$. In contrast, $[Ca^{2+}]$ gradients will typically produce substantially smaller $[H^+]$ gradients because $Ca^{2+}$ buffers with high $S_{H:Ca}$ (e.g., HDPs) carry only a small fraction of diffusive $Ca^{2+}$ flux (i.e., $\alpha_{Ca} << 1$; HDPs hold 1% of total cytoplasmic $Ca^{2+}$).

We have further tested the $Ca^{2+}/H^+$ buffer hypothesis by comparing experimental data with predictions of a diffusion-reaction model (*Mathematical Supplement*). This features pH-sensitive $Ca^{2+}$ binding to large, essentially immobile $Ca^{2+}$ buffers (troponin, calmodulin, and SERCA), plus smaller mobile ATP and HDP molecules (Table S1). The model can be used to simulate $[Ca^{2+}]_i$ within a myocyte during an imposed longitudinal $[H^+]_i$ gradient of 0.6 $pH_i$ units, as attained experimentally (Fig. 4). The presence of immobile buffers alone predicts an initial $[Ca^{2+}]_i$ rise in the acidic zone of the cell, but this dissipates by means of diffusion. A sustained $Ca^{2+}$ rise, however, occurs when ATP (7.5 mM) is included in the model and, to a much greater extent, when HDPs (17 mM) are included (Fig. 6*B*). A combination of the two mobile buffers accurately simulates the experimentally observed sustained $[Ca^{2+}]_i$ gradient (Fig. 6*B*). The diffusion-reaction model predicts attenuation of the $Ca^{2+}$ gradient on elevation of $[Mg^{2+}]_i$ (Fig. 6*C*) or on adding metabolic inhibitors that deplete $ATP_i$ with a concurrent rise in $[Mg^{2+}]_i$ (Fig. 6*C*). Finally, the model predicts that a localized cytoplasmic region of metabolic stress will induce a sustained local rise of both $[Ca^{2+}]_i$ and $[H^+]_i$ (Fig. 6*D*), again as observed experimentally (Fig. 5C). The localization and stabilization of $H^+$ and $Ca^{2+}$ microdomains via spatial cytoplasmic $Ca^{2+}/H^+$ exchange are thus supported both experimentally and theoretically.

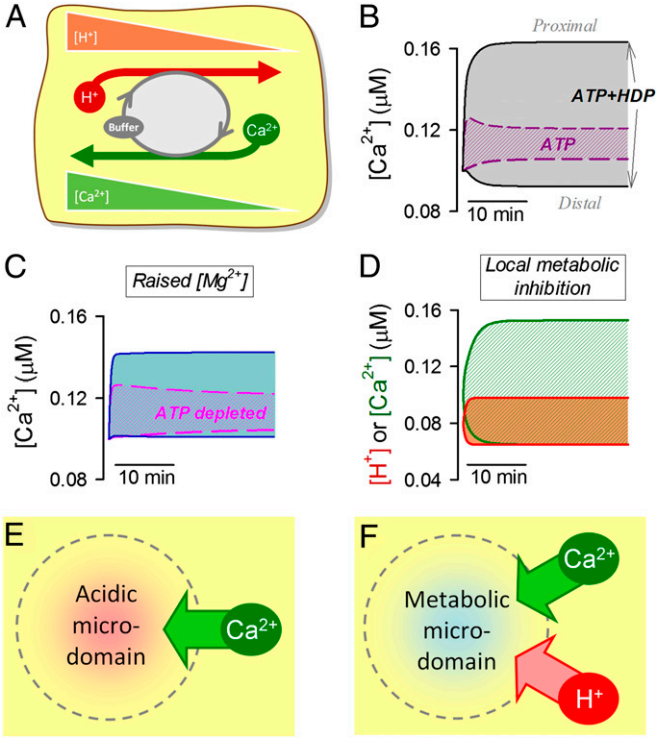


**Fig. 6.** Modeling cytoplasmic $Ca^{2+}/H^+$ exchange. Acidic microdomains actively recruit $Ca^{2+}$ ions, and metabolic microdomains recruit both $Ca^{2+}$ and $H^+$ ions. (*A*) Cartoon shows the role of mobile $Ca^{2+}/H^+$ buffers (i.e., HDPs, ATP) in producing and sustaining $[Ca^{2+}]_i$ nonuniformity, generated by a longitudinal $[H^+]$ gradient (or vice versa). (*B*) Mathematical model simulates $[Ca^{2+}]_i$ at either end of a model myocyte during an imposed $[H^+]$ gradient (pH 6.5 at the proximal end and pH 7.2 at the distal end). Simulation with 7.5 mM ATP (dashed line) or 7.5 mM ATP and 17 mM HDP (solid line). HDP and ATP are able to support a standing $[Ca^{2+}]$ gradient during imposed $[H^+]$ nonuniformity. (*C*) Simulation with 7.5 mM ATP plus 17 mM HDP when $[Mg^{2+}]_i$ is raised fourfold (solid line) or when ATP is depleted and $[Mg^{2+}]_i$ is raised by 7 mM (dashed line). $[Ca^{2+}]$ gradients are greatly reduced. (*D*) Simulation with 17 mM HDP. One-half of the cell is a net consumer of ATP (15 mM/min) and the other half a net producer of ATP (15 mM/min); the cell-averaged concentration [ATP] is 7.5 mM. Standing $[Ca^{2+}]$ and $[H^+]$ gradients develop. (*E*) Local acidic microdomain will recruit $Ca^{2+}$ via cytoplasmic $Ca^{2+}/H^+$ exchange. (*F*) Metabolic microdomain (i.e., local zone of net MgATP hydrolysis) will recruit both $Ca^{2+}$ and $H^+$ ions.

**Physiological Importance of $Ca^{2+}/H^+$ Coupling and the Cytoplasmic $Ca^{2+}/H^+$ Exchanger.** The ability of cytoplasmic buffers to raise diastolic $[Ca^{2+}]_i$ rapidly in response to a rise of $[H^+]_i$ has important implications for cardiac function. Because $H^+$ ions are end products of metabolism, cytoplasmic $Ca^{2+}/H^+$ coupling may provide an efficient means of matching metabolic activity with an appropriate basal $Ca^{2+}$ signal. Many $Ca^{2+}$-activated cellular process, such as excitation, contraction, and gene transcription, are inhibitable by $H^+$ ions; thus, a positive coupling between $[H^+]$ and diastolic $[Ca^{2+}]$ will help to sustain $Ca^{2+}$ activation in the face of a metabolic challenge. Additional effects of acidosis on dynamic $Ca^{2+}$ signaling, routed through NHE and NCX activity, have been well

characterized (7, 8), but these latter effects will be superimposed on the $H^+$-activated control of diastolic $Ca^{2+}$ described here.

The strong spatial coupling between $[H^+]_i$ and $[Ca^{2+}]_i$ in cardiac myocytes implies that any localized $H^+$ microdomain has the potential to generate an overlying $Ca^{2+}$ microdomain (shown schematically in Fig. 6*E*). Spatial $pH_i$ gradients of 0.1–0.2 $pH_i$ units can be generated in myocytes by sarcolemmal NHE activity (4, 13, 33), and Eq. **1** suggests that these will be associated with a $[Ca^{2+}]_i$ gradient of 30–60 nM (note that the cytoplasmic $Ca^{2+}/H^+$ exchanger's $V_{max}$ increases with sharper $pH_i$ gradients over shorter distances). Cytoplasmic $Ca^{2+}/H^+$ exchange could enhance the transport of $Ca^{2+}$ toward mitochondria, where a local $[H^+]$ gradient [~0.5 pH units (34)] stretches from the acidic intermembrane space (IMS) to the more alkaline cytoplasmic domain. The IMS is readily accessed by ATP and other small buffer molecules (35), implying that diffusible $Ca^{2+}/H^+$ exchange may promote an uphill flux of cytoplasmic $Ca^{2+}$ into this region, thereby facilitating mitochondrial $Ca^{2+}$ uptake via the uniporter. Spatial gradients of $pH_i$ in the heart may also arise from regional differences in metabolic rate and capillary perfusion (4). For example, under localized ischemia, extracellular gradients of membrane-permeant weak acids ($CO_2$ and lactic acid) will generate large and sustained standing gradients of $pH_i$ (14), which are likely to extend over many cell lengths in the myocardium. Because HDPs and ATP permeate gap junctions (36), $pH_i$ gradients between electrically coupled cells would then be expected to drive uphill, cell-to-cell $Ca^{2+}$ flux into the acidic region, via cytoplasmic $Ca^{2+}/H^+$ exchange over a wider spatial range.

Cytoplasmic domains of elevated $[Ca^{2+}]$ may drive an uphill $H^+$ flux, provided the local $[Ca^{2+}]$ gradient is of sufficient magnitude and persistence. Cyclical $Ca^{2+}$ release events locally raise dyadic $[Ca^{2+}]$ into the high micromolar range (37), which is predicted to reduce [MgATP] and $[ATP^{2-}]$ and to raise [CaATP] (37, 38). A similar redistribution of buffer states is expected for HDPs. Consequently, SR $Ca^{2+}$ release, by raising dyadic $[Ca^{2+}]$, may drive local $Ca^{2+}/H^+$ exchange, thereby elevating dyadic $[H^+]$ and possibly influencing RyR gating. Because rapid pH responses will be smoothed by high overall cytoplasmic $H^+$ buffering, cyclical changes in dyadic $[Ca^{2+}]$ may translate into a more tonic dyadic $[H^+]$ rise. For example, a time-averaged dyadic $[Ca^{2+}]$ of 50 μM could raise $[H^+]$ by 1 μM if HDPs were responsible for mediating 1% of passive $Ca^{2+}$ efflux out of the dyad (Eq. **2**).

A further degree of complexity is introduced by the sensitivity of cytoplasmic $Ca^{2+}/H^+$ exchange to the cell's metabolic state, through dynamic changes in ATP concentration and related changes in $[Mg^{2+}]_i$. Indeed, localized $ATP_i$ depletion (metabolic stress, either within a cell or regionally within the myocardium), by acting on the $Ca^{2+}/H^+$ exchange mechanism (compare with Fig. 5*C*), may contribute to the elevated levels of intracellular $Ca^{2+}$ and $H^+$ typically observed in localized ischemia (Fig. 6*F*).

Mobile $Ca^{2+}/H^+$ buffers are not unique to the heart; thus, many other cell types are likely to show spatial $Ca^{2+}/H^+$ exchange reactions. ATP is a universal molecule present in all cells, and HDPs are present at high concentrations in skeletal muscle (20), glia, and neurons (39). Furthermore, in addition to cardiac myocytes (4, 13, 14), spatial $pH_i$ nonuniformity has been reported, at least transiently, in epithelial cells (40), glia (41), migrating tumor cells (42), and molluscan and mammalian neurons (43, 44), whereas membrane acid transport has been reported to generate $pH_i$ microdomains in heterologous expression systems (45). In some cases, these $pH_i$ microdomains have been associated with local $Ca^{2+}$ gradients (43). We have thus demonstrated a spatial paradigm linking the behavior of intracellular $H^+$ and $Ca^{2+}$, likely to be of fundamental importance in the control of cell signaling and function.

## Materials and Methods

**Isolation of Ventricular Myocytes and Mitochondria.** Enzymic isolation of myocytes from rat heart ventricles was performed using a previously published method (14). Animals were killed by means of schedule I killing, as approved by the UK Home Office and departmental guidelines (Department of Physiology, Anatomy and Genetics, Oxford). Mitochondrial isolation was performed according to the method of Bednarczyk et al. (46).

**Solutions.** Normal Tyrode solution: 140 mM NaCl, 4.5 mM KCl, 1 mM $CaCl_2$, 1 mM $MgCl_2$, 11 mM glucose, 10 mM Hepes (pH 7.4) at 37 °C. 0Na-0Ca solution: $Na^+$ replaced with 140 mM *N*-methyl-D-gluconate and $CaCl_2$ replaced with 0.5 mM EGTA. Pipette-filling solution: 110 mM KCl, 5 mM NaCl, 5 mM MgATP, 5 mM phosphocreatine, 1 mM NaGTP, and 10 mM Hepes (titrated to pH 7.2 with 1 M KOH). High-$K^+$ "intracellular solution" for superfusing permeabilized cells: 100 mM K-aspartate, 30 mM KCl, 15 mM Hepes, 1 or 5 mM EGTA, 0.5 mM pyruvate, 0.5 mM malate, 0.25 mM K-ADP, 5 mM Mg-ATP, 5 mM Na-phosphocreatine, 0.5 mM K-phosphate, and 4% (wt/vol) dextran (pH at 6.6 or 7.2), and $[Ca^{2+}]$ and $[Mg^{2+}]$ were adjusted appropriately using CaBuf software (G. Droogmans, Leuven, Belgium). Acetate-containing solutions had equivalently reduced $Cl^-$. Total $Ca^{2+}$ in $Ca^{2+}$-containing acetate solutions was raised ~20% to compensate for $Ca^{2+}$-acetate binding ($[Ca^{2+}]_i$ measured by electrode). Bathing solution for mitochondria: 140 mM KCl, 2 mM malate, 2 mM glutamate, 10 mM Hepes (pH 7.2), 1 mM $MgCl_2$, and 10 μM BAPTA (sparingly low $Ca^{2+}$ buffering to improve resolving power of dye to detect $Ca^{2+}$ release), and measured $[Ca^{2+}]_i$ at pH 7.2 was 130 nM (based on calibration of FuraRed fluorescence). High $K^+$ buffer for resuspending mitochondria: 140 mM KCl, 10 mM Hepes, 1 mM EGTA, and 1 mM $MgCl_2$ (pH 7.2).

**Superfusion, Dual Microperfusion, and Fluorescence Imaging of Myocytes.** AM loading of dyes or buffers was performed in nonsuperfused solution at room temperature. Superfusion (37 °C) was performed in Perspex chambers mounted on a Leica TCS NT confocal imaging microscope (14). Dual microperfusion was performed on myocytes at a right angle to the microstream boundary using a previously published method (14). One microstream contained, in addition, 15 mM sucrose to help visualize the interstream boundary. Intracellular fluorescence was measured with the following settings: cSNARF1 (10-min loading): excitation at 514 nm, emission at 580 nm and 640 nm; Fluo3 and MagFluo4 (5-min loading): excitation at 488 nm, emission at >520 nm; Indo1 (30-min loading): excitation at 361 nm, emission at 405 nm and 465 nm; and Rhod2: excitation at 514 nm and emission at 580 nm. The Fluo3 $K_d$ was estimated in situ to be 0.84 μM by pipette-loading cells with 10 μM to measure maximal fluorescence ($F_{max}$) relative to $F_0$ ($F_{max}/F_0 = 9.3 \pm 0.3$). For simultaneous Indo1/cSNARF1 measurements, cSNARF1 fluorescence was corrected for Indo1 bleed-through. The $pH_i$ in intact cells was calibrated using nigericin (10 μM). $Ca^{2+}$ measured in permeabilized cells with Rhod2 was calibrated with ionomycin (10 μM).

**Fluorimetry on Mitochondrial Suspensions.** Mitochondria (1–2 g of protein per liter) were AM-loaded with Indo1 (20 μM for 20 min) to measure matrix $[Ca^{2+}]$ and then resuspended in Indo1-free media containing FuraRed (20 μM free acid) to measure extramitochondrial $[Ca^{2+}]$. The measurement artifact associated with the pH change was established in mitochondria-free solutions and subtracted from mitochondria-containing recordings. Indo1 was measured at an excitation of 340 nm and emission of 410 and 490 nm; FuraRed was measured at an excitation of 430 and 460 nm and an emission of 615 nm. Measurements performed on a Hitachi F4500 fluorescence spectrophotometer.

**Myocyte Permeabilization.** Cell surface membrane permeabilization was performed by a 15-s exposure to 0.005% saponin in high-$K^+$ internal solution. Cells were subsequently superfused with intracellular solution.

**Photolytic UV Uncaging of Acid.** The photolabile donor NBA in ethanol stock was dissolved in solutions at 1–5 mM. Uncaging was triggered with 361-nm laser-line (18) scanning at 400 Hz.

**In Vitro Assays for $H^+/Ca^{2+}$ Buffers.** Solutions were based on 140 mM KCl, 5 mM NBA, 10 mM Hepes, and 150 μM BAPTA to buffer background $Ca^{2+}$. Solutions were prepared at a 200% concentration, warmed to 40 °C, and mixed 1:1 with warm 2% low-gelling-point agarose solution. They were then allowed to cool and set on coverslips (10 μL) for uncaging and $pH/Ca^{2+}$ imaging.

**ACKNOWLEDGMENTS.** This study was funded by British Heart Foundation Programme Grant RG/08/016 (to R.D.V.-J.), by National Institutes of Health Grant 5R37HL042873 (to K.W.S.), and by a fellowship from the Royal Society (to P.S.). We thank Dr. Alzbeta Hulikova for performing the ATP assays and Dr. Robert Wilkins for access to the spectrophotometer.

1. Clapham DE (2007) Calcium signaling. *Cell* 131(6):1047–1058.
2. Boron WF (2004) Regulation of intracellular pH. *Adv Physiol Educ* 28(1-4):160–179.
3. Bers DM (2002) Cardiac excitation-contraction coupling. *Nature* 415(6868):198–205.
4. Vaughan-Jones RD, Spitzer KW, Swietach P (2009) Intracellular pH regulation in heart. *J Mol Cell Cardiol* 46(3):318–331.
5. Mandel F, Kranias EG, Grassi de Gende A, Sumida M, Schwartz A (1982) The effect of pH on the transient-state kinetics of $Ca^{2+}$-$Mg^{2+}$-ATPase of cardiac sarcoplasmic reticulum. A comparison with skeletal sarcoplasmic reticulum. *Circ Res* 50(2):310–317.
6. Choi HS, Trafford AW, Orchard CH, Eisner DA (2000) The effect of acidosis on systolic Ca2+ and sarcoplasmic reticulum calcium content in isolated rat ventricular myocytes. *J Physiol* 529(Pt 3):661–668.
7. Bountra C, Vaughan-Jones RD (1989) Effect of intracellular and extracellular pH on contraction in isolated, mammalian cardiac muscle. *J Physiol* 418:163–187.
8. Harrison SM, Frampton JE, McCall E, Boyett MR, Orchard CH (1992) Contraction and intracellular $Ca^{2+}$, $Na^+$ and $H^+$ during acidosis in rat ventricular myocytes. *Am J Physiol* 262(2 Pt 1):C348–C357.
9. Gambassi G, et al. (1993) Effects of acidosis on resting cytosolic and mitochondrial Ca2+ in mammalian myocardium. *J Gen Physiol* 102(3):575–597.
10. Kushmerick MJ, Podolsky RJ (1969) Ionic mobility in muscle cells. *Science* 166(3910): 1297–1298.
11. Vaughan-Jones RD, Peercy BE, Keener JP, Spitzer KW (2002) Intrinsic H(+) ion mobility in the rabbit ventricular myocyte. *J Physiol* 541(Pt 1):139–158.
12. Bassani RA, Bassani JW, Bers DM (1992) Mitochondrial and sarcolemmal $Ca^{2+}$ transport reduce $[Ca^{2+}]_i$ during caffeine contractures in rabbit cardiac myocytes. *J Physiol* 453:591–608.
13. Swietach P, Vaughan-Jones RD (2005) Spatial regulation of intracellular pH in the ventricular myocyte. *Ann N Y Acad Sci* 1047:271–282.
14. Swietach P, Leem CH, Spitzer KW, Vaughan-Jones RD (2005) Experimental generation and computational modeling of intracellular pH gradients in cardiac myocytes. *Biophys J* 88(4):3018–3037.
15. Cheng H, Lederer WJ, Cannell MB (1993) Calcium sparks: Elementary events underlying excitation-contraction coupling in heart muscle. *Science* 262(5134): 740–744.
16. Higgins ER, Cannell MB, Sneyd J (2006) A buffering SERCA pump in models of calcium dynamics. *Biophys J* 91(1):151–163.
17. Jiang D, Zhao L, Clapham DE (2009) Genome-wide RNAi screen identifies Letm1 as a mitochondrial $Ca^{2+}/H^+$ antiporter. *Science* 326(5949):144–147.
18. Swietach P, Spitzer KW, Vaughan-Jones RD (2007) pH-Dependence of extrinsic and intrinsic H(+)-ion mobility in the rat ventricular myocyte, investigated using flash photolysis of a caged-H(+) compound. *Biophys J* 92(2):641–653.
19. Cordeiro JM, et al. (2001) Location of the initiation site of calcium transients and sparks in rabbit heart Purkinje cells. *J Physiol* 531(Pt 2):301–314.
20. O'Dowd JJ, Robins DJ, Miller DJ (1988) Detection, characterisation, and quantification of carnosine and other histidyl derivatives in cardiac and skeletal muscle. *Biochim Biophys Acta* 967(2):241–249.
21. House JR, Miller DJ, O'Dowd JJ (1989) Differences in the distribution of the imidazoles of rat heart between atria and ventricles. *J Physiol* 417:162P.
22. Swietach P, Vaughan-Jones RD (2005) Relationship between intracellular pH and proton mobility in rat and guinea-pig ventricular myocytes. *J Physiol* 566(Pt 3): 793–806.
23. O'Dowd JJ, Cairns MT, Trainor M, Robins DJ, Miller DJ (1990) Analysis of carnosine, homocarnosine, and other histidyl derivatives in rat brain. *J Neurochem* 55(2): 446–452.
24. Brini M, Carafoli E (2009) Calcium pumps in health and disease. *Physiol Rev* 89(4): 1341–1378.
25. Swietach P, Camelliti P, Hulikova A, Kohl P, Vaughan-Jones RD (2010) Spatial regulation of intracellular pH in multicellular strands of neonatal rat cardiomyocytes. *Cardiovasc Res* 85(4):729–738.
26. Baran EJ (2000) Metal complexes of carnosine. *Biochemistry (Mosc)* 65(7):789–797.
27. Almulla HA, Bush PG, Steele MG, Ellis D, Flatman PW (2006) Loading rat heart myocytes with $Mg^{2+}$ using low-$[Na^+]$ solutions. *J Physiol* 575(Pt 2):443–454.
28. Lazdunski M, Frelin C, Vigne P (1985) The sodium/hydrogen exchange system in cardiac cells: Its biochemical and pharmacological properties and its role in regulating internal concentrations of sodium and internal pH. *J Mol Cell Cardiol* 17(11): 1029–1042.
29. Bers DM, Ellis D (1982) Intracellular calcium and sodium activity in sheep heart Purkinje fibres. Effect of changes of external sodium and intracellular pH. *Pflugers Arch* 393(2):171–178.
30. Kohmoto O, Spitzer KW, Movsesian MA, Barry WH (1990) Effects of intracellular acidosis on $[Ca^{2+}]_i$ transients, transsarcolemmal $Ca^{2+}$ fluxes, and contraction in ventricular myocytes. *Circ Res* 66(3):622–632.
31. Kushmerick MJ (1997) Multiple equilibria of cations with metabolites in muscle bioenergetics. *Am J Physiol* 272(5 Pt 1):C1739–C1747.
32. Minta A, Kao JP, Tsien RY (1989) Fluorescent indicators for cytosolic calcium based on rhodamine and fluorescein chromophores. *J Biol Chem* 264(14):8171–8178.
33. Garciarena CD, Ma YL, Swietach P, Huc L, Vaughan-Jones RD (2013) Sarcolemmal localisation of $Na^+/H^+$ exchange and $Na^+$-$HCO_3^-$co-transport influences the spatial regulation of intracellular pH in rat ventricular myocytes. *J Physiol*, jphysiol.2012.249664.
34. Xiong JW, Zhu L, Jiao X, Liu SS (2010) Evidence for DeltapH surface component (DeltapH(S)) of proton motive force in ATP synthesis of mitochondria. *Biochim Biophys Acta* 1800(3):213–222.
35. Yurkov VI, Fadeeva MS, Yaguzhinsky LS (2005) Proton transfer through the membrane-water interfaces in uncoupled mitochondria. *Biochemistry (Mosc)* 70(2): 195–199.
36. Swietach P, Rossini A, Spitzer KW, Vaughan-Jones RD (2007) $H^+$ ion activation and inactivation of the ventricular gap junction: A basis for spatial regulation of intracellular pH. *Circ Res* 100(7):1045–1054.
37. Cannell MB, Kong CH (2012) Local control in cardiac E-C coupling. *J Mol Cell Cardiol* 52(2):298–303.
38. Valent I, Zahradníková A, Pavelková J, Zahradník I (2007) Spatial and temporal $Ca^{2+}$, $Mg^{2+}$ and $ATP^{2-}$ dynamics in cardiac dyads during calcium release. *Biochim Biophys Acta* 1768(1):155–166.
39. Biffo S, Grillo M, Margolis FL (1990) Cellular localization of carnosine-like and anserine-like immunoreactivities in rodent and avian central nervous system. *Neuroscience* 35(3): 637–651.
40. Stewart AK, Boyd CA, Vaughan-Jones RD (1999) A novel role for carbonic anhydrase: Cytoplasmic pH gradient dissipation in mouse small intestinal enterocytes. *J Physiol* 516(Pt 1):209–217.
41. Ro HA, Carson JH (2004) pH microdomains in oligodendrocytes. *J Biol Chem* 279(35): 37115–37123.
42. Martin C, Pedersen SF, Schwab A, Stock C (2011) Intracellular pH gradients in migrating cells. *Am J Physiol Cell Physiol* 300(3):C490–C495.
43. Schwiening CJ, Willoughby D (2002) Depolarization-induced pH microdomains and their relationship to calcium transients in isolated snail neurones. *J Physiol* 538(Pt 2): 371–382.
44. Willoughby D, Schwiening CJ (2002) Electrically evoked dendritic pH transients in rat cerebellar Purkinje cells. *J Physiol* 544(Pt 2):487–499.
45. Johnson DE, Casey JR (2011) Cytosolic H+ microdomain developed around AE1 during AE1-mediated $Cl^-/HCO_3^-$ exchange. *J Physiol* 589(Pt 7):1551–1569.
46. Bednarczyk P, Barker GD, Halestrap AP (2008) Determination of the rate of K(+) movement through potassium channels in isolated rat heart and liver mitochondria. *Biochim Biophys Acta* 1777(6):540–548.